








Research article

# Eco-friendly approach for nanocellulose isolation from agricultural wastes and the fabrication of bioaerogel scaffolds

Rahadian Zainul<sup>1</sup>, Yonss Mbrook Albadn<sup>2</sup>, Esam Bashir Yahya<sup>3,4\*</sup>, Salim Manoharadas<sup>5</sup>,  
Nur Izzaati Saharudin<sup>2,4</sup>, Abdul Khalil H. P. S.<sup>2,4</sup>, Mohammad Rizwan Khan<sup>6</sup>,  
Mohamed Jaber<sup>7</sup>

<sup>1</sup>Department of Chemistry, Faculty of Mathematics and Natural Sciences, Universitas Negeri Padang, Indonesia

<sup>2</sup>Bioresource Technology Division, School of Industrial Technology, Universiti Sains Malaysia, 11800 Penang, Malaysia

<sup>3</sup>Bioprocess Technology Division, School of Industrial Technology, Universiti Sains Malaysia, 11800 Penang, Malaysia

<sup>4</sup>Green Biopolymer, Coatings and Packaging Cluster, School of Industrial Technology, Universiti Sains Malaysia, 11800 Penang, Malaysia

<sup>5</sup>Department of Botany and Microbiology, College of Science, King Saud University, P.O. BOX 2454, Riyadh, Saudi Arabia

<sup>6</sup>Department of Chemistry, College of Science, King Saud University, 11451 Riyadh, Saudi Arabia

<sup>7</sup>Department of Mathematical Science, College of Engineering and Science, Florida Institute of Technology, USA

Received 13 November 2023; accepted in revised form 15 December 2023

**Abstract.** In this study, we employed supercritical carbon dioxide (scCO<sub>2</sub>) treatment under varying conditions: low-pressure treatment at 30 MPa and high temperature at 80 °C (LPHT group) and high-pressure treatment at 60 MPa and low temperature at 50 °C (HPLT group) for nanocellulose isolation. The scCO<sub>2</sub> treatment resulted in smaller particle sizes and enhanced crystallinity. Notably, HPLT exhibited superior efficiency compared to LPHT treatment. Utilizing temperatures and pressures above the critical point effectively penetrated natural fibers, reducing nanocellulose particle sizes. Moreover, high-pressure and low-temperature nanocellulose demonstrated the highest crystallinity and negative zeta potential values (78.2% and –32.4±4.01 mV), surpassing those of the low-pressure and high-temperature group (77.9% and 26.0±2.34 mV) and control (77.3% and 25.9±3.13 mV). The concentration of nanocellulose significantly impacted the porosity, pore size, and water absorption of the bioaerogel scaffolds, indicating the potential for sustainable and environmentally friendly approaches in material fabrication for diverse applications.

**Keywords:** oil palm empty fruit bunch, nanocellulose, supercritical treatment, isolation, cleaner approach

## 1. Introduction

Over the past two decades, global population growth has underscored the imperative for smart, sustainable approaches in utilizing everyday materials. Empty fruit bunches (EFBs) stand as a primary by-product of the palm oil milling process. Following the harvesting and processing of palm oil fruits, sterilization

and subsequent separation steps yield the empty fruit bunches, comprising fibrous materials like stalks, fronds, and residual palm fruit [1]. Traditionally considered waste, these empty fruit bunches were often disposed of or incinerated, leading to environmental degradation and contributing to greenhouse gas emissions [2]. However, recent years have witnessed

\*Corresponding author, e-mail: [essam912013@gmail.com](mailto:essam912013@gmail.com)

© BME-PT

a shift toward exploring sustainable applications for EFBs, aiming to curtail waste and foster a circular economy within the palm oil industry.

EFBs have found extensive use in producing nanocellulose, a form of cellulose processed into minute particles [3]. Renowned for its exceptional characteristics like remarkable strength, extensive surface area, and biodegradability nanocellulose stands as a promising material for diverse applications spanning textiles, packaging, cosmetics, and biomedicine [4–6]. The increasing emphasis on sustainable development has notably spurred the evolution of new isolation and fabrication methods that employ cleaner approaches, involving minimal or no chemical usage. Mechanical methods have been employed, involving the physical breakdown of cellulose fibers to nanoscale dimensions. Alternatively, chemical techniques dissolve cellulose fibers, followed by nanocellulose precipitation or regeneration [7]. Both approaches yield nanocellulose with varying properties, tailored to specific applications. Aerogel, an ultralight solid material formed from a gel with its liquid component replaced by gas [8], boasts remarkable properties that render it highly valuable across various applications [9].

Nanocellulose aerogel, derived from nanoscale cellulose particles [10], merges the distinct attributes of aerogels and nanocellulose, forming a lightweight material with exceptional mechanical robustness, high porosity, and thermal insulation capabilities [11, 12]. Its versatile properties render nanocellulose aerogels ideal for diverse applications in tissue engineering, drug delivery systems, and wound healing, given their biocompatibility, adjustable porosity, and support for cell growth and tissue regeneration. These aerogels, with their heightened surface area and porosity, demonstrate effectiveness in adsorbing and eliminating pollutants—ranging from heavy metals to organic compounds—in water and air, presenting potential uses in environmental remediation and water purification [4, 13]. This study aimed to streamline the chemical requirements in the nanocellulose isolation process from empty fruit bunches by integrating  $\text{scCO}_2$  into the extraction method. Furthermore, the investigation delved into the supercritical treatment's mechanism to evaluate the impact of heat and pressure on the fiber fraction. Optimal nanocellulose, exhibiting desired properties, was then employed to create nanocellulose aerogels with varied concentrations to assess the effect of nanocellulose concentration on aerogel properties.

## 2. Experimental section

### 2.1. Materials

Empty fruit bunches were procured from N.T.P.M SDN BHD (Penang, Malaysia), while Supercritical Carbon Dioxide was sourced from ZARM Scientific (Selangor, Malaysia). All chemicals utilized in this study, of analytical grade, were obtained from Sigma-Aldrich (Schnelldorf, Germany) and used without additional purification.

### 2.2. Characterization of raw empty fruit bunch fibers

The fibers collected underwent analysis prior to experimentation to determine their moisture content. Additionally, chemical analysis for holocellulose, lignin, and ash content was conducted using the standardized Technical Association of the Pulp and Paper Industry (TAPPI) methods [14, 15].

### 2.3. Isolation of nanocellulose

The nanocellulose isolation from empty fruit bunches followed a method adapted from [16] and [17], with certain modifications, and an original method was employed as a control. Initially, raw empty fruit bunches were fragmented into pieces smaller than 10 mm, washed thoroughly, and subjected to heat treatment in an alkaline solution containing 12.5 wt% NaOH at 180 °C for 4 h using a digester. The resulting alkali-treated fibers underwent multiple washes and then underwent chlorine-free bleaching by treatment with 1.5%  $\text{H}_2\text{O}_2$ , 1.5% NaOH, and 0.25%  $\text{MgSO}_4$  at 80 °C for 3 h. These bleached fibers were divided into different treatment groups: low pressure-high temperature (30 MPa at 80 °C) denoted as LPHT, high pressure-low temperature (60 MPa at 50 °C) known as HPLT, and a control group (C) that did not undergo supercritical treatment. For the C group, after pulping and bleaching, mild acid hydrolysis using a low concentration (3%) of oxalic acid was applied for 1 h. The resulting samples were thoroughly washed to neutralize the pH and further processed via high-pressure homogenization using an OV5 homogenizer (Velp Scientifica, Usmate Velate MB, Italy) for 6 h at power 4 (12 000 rpm) before refrigeration for subsequent use.

### 2.4. Characterization of nanocellulose

Particle size analysis of the cellulose nanofibers was conducted using a laser diffraction analyzer (Nano-ZS90, Malvern, UK). The experiment was replicated

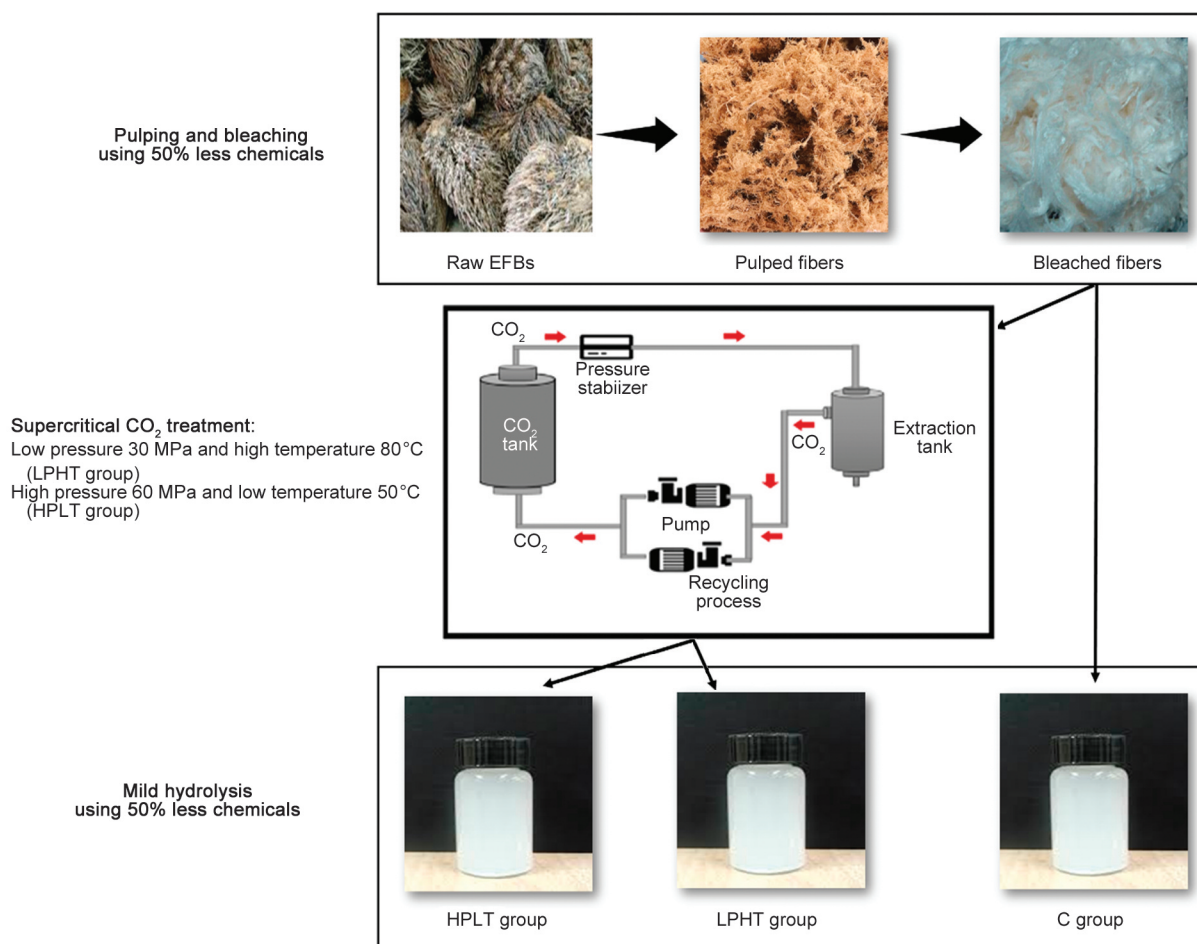


**Figure 1.** Isolation steps of nanocellulose from raw oil palm empty fruit bunch.

three times, and the mean value was considered as the outcome. To investigate the surface functional groups, FT-IR spectroscopy (Nicolet I S10 spectrometer, Thermo Fisher Scientific Inc., Madison, USA) was employed, covering a spectral range of 4000 to 400  $\text{cm}^{-1}$  with a scanning precision of 4  $\text{cm}^{-1}$ . The FTIR-ATR analysis served to confirm the chemical composition of the nanocellulose. The structural and crystalline properties were examined using X-ray diffractometry (XRD) following the procedures outlined in [18]. Additionally, thermal analysis of the cellulose nanofibers was performed using a TGA and DTG analyzer (TGA/SDTA 851e, (Mettler Toledo Corporation, Greifensee, Switzerland) with a constant heating range of 25 to 800 °C at 10 °C/min<sup>-1</sup>.

## 2.5. Fabrication of bioaerogel scaffolds

Bioaerogel scaffold samples, labeled as BAS1, BAS1.5, BAS2, and BAS2.5, were prepared by suspending different concentrations (1, 1.5, 2, and 2.5%) of the isolated cellulose nanofibers in distilled water. The fabrication process involved homogenizing

each sample for an additional 6 hours, followed by immediate freezing overnight and subsequent lyophilization for a duration of 3 days (Figure 1). The resulting bioaerogels were stored in a desiccator until further utilization.

## 2.6. Characterization of bioaerogel scaffolds

Morphological characterization of the bioaerogels was conducted using a High-Resolution Scanning Electron Microscope (50 VP, Carl Zeiss Group, Oberkochen, Germany). Thin layers of the samples were prepared by cutting them with a sharp blade and directly examined under the electron microscope. The analysis of surface functional groups, thermogravimetric analysis, differential scanning calorimetry, and crystallinity analysis of the bioaerogels were carried out using the same equipment utilized for nanocellulose characterization. The mechanical properties of the bioaerogel scaffolds were investigated through Texture Profile Analysis using a TA-HDi textile analyzer machine (Stable Micro Systems, Surrey, UK) [5]. Standardized sample sizes

measuring  $2 \times 2 \times 1$  cm (length  $\times$  width  $\times$  height) underwent two compression cycles, each reducing their height to 75% of the initial measurement. Texture profile analyses were conducted during these compression cycles, evaluating parameters such as hardness, cohesiveness, resilience, gumminess, springiness, and chewiness.

The porosity of the samples was measured by cutting the aerogels into constant shapes of  $1 \text{ cm}^3$ , and then bulk density was calculated from the shape and weight. The Equation (1) was then used to calculate the porosity:

$$\text{Porosity [\%]} = 1 - \frac{\text{aerogel density}}{\text{bulk density}} \cdot 100 \quad (1)$$

The surface area of all the samples was determined using the Brunauer–Emmett–Teller (BET) analysis, which quantified the nitrogen adsorption at various relative vapor pressures, following the methodology outlined in the work of Sai *et al.* [19]. Water absorption capacity of the samples was also calculated by cropping constant dimensions of the samples immersing them separately in 20 ml of distilled water

and keep them to saturate for 5 min. The excessive amount of water was then removed from the saturated samples by filter paper and the average weight was determined.

### 3. Results and discussion

#### 3.1. Characterization of raw oil palm empty fruit bunch fibers and isolated nanocellulose

The average moisture content of empty fruit bunches measured at  $(11.6 \pm 0.4\%)$  may vary due to factors like climate, harvest timing, and storage conditions [20]. Maintaining proper moisture levels during fiber processing and storage is crucial to preserve their mechanical properties and prevent damage caused by microbial growth. Excessive moisture can facilitate bacterial and fungal growth, resulting in fiber deterioration and reduced strength [21].

Holocellulose represents the carbohydrate fraction in biomass, encompassing the total polysaccharide fraction after lignin removal [22]. In this study, raw empty fruit bunch fibers contained  $(74.7 \pm 3.2\%)$  cellulose and  $(11.4 \pm 0.8\%)$  hemicellulose, with lignin

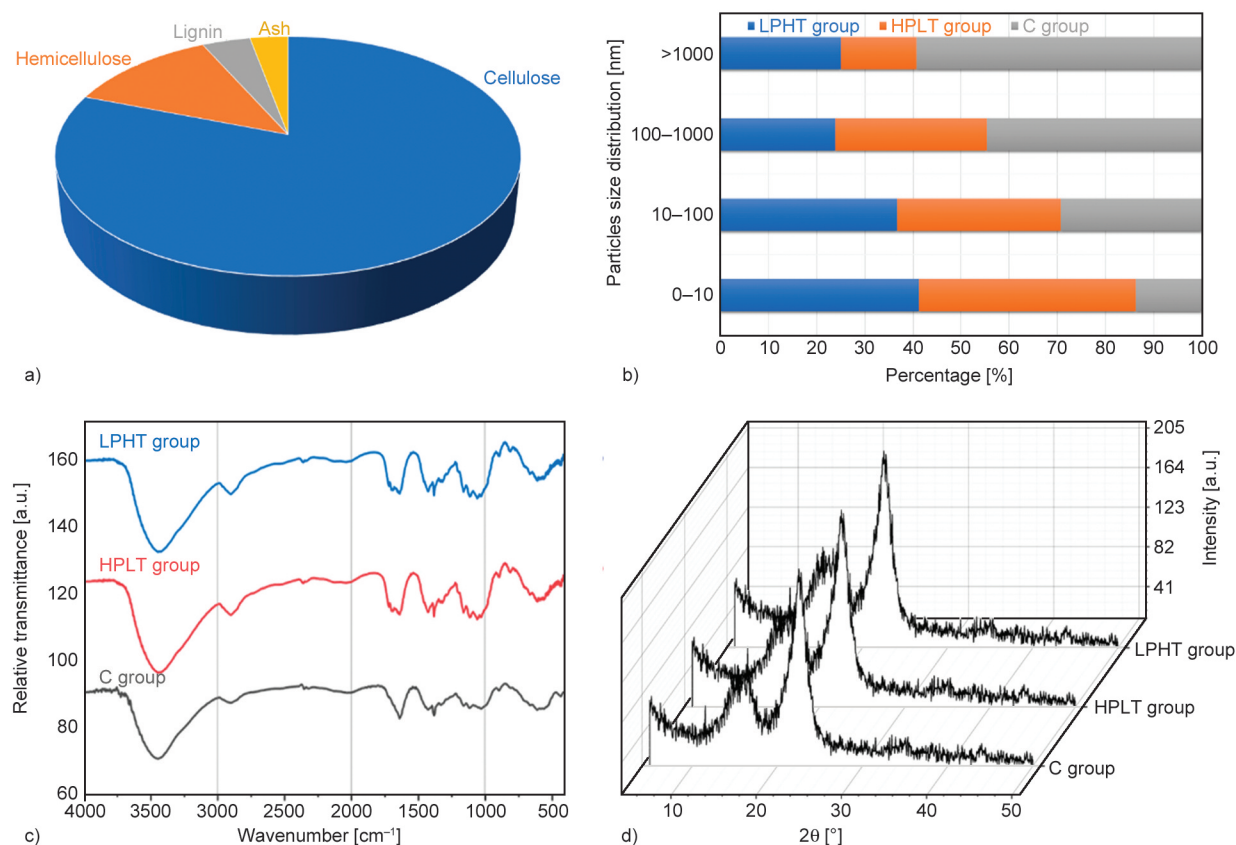


**Figure 2.** Characterization of oil palm empty fruit bunch fibers and the isolated nanocellulose; a) chemical composition of raw fibers, b) particle size distribution of isolated nanocellulose, c) FT-IR spectra, and d) XRD analysis of isolated nanocellulose.



and ash comprising ( $3.7 \pm 0.6$  %) and ( $2.9 \pm 0.9$  %) respectively (Figure 2a). Compared to previous studies reporting lower cellulose content, these findings highlight empty fruit bunches as an exceptional source of nanocellulose. Chemical analysis results of the raw fibers and isolated nanocellulose properties are depicted in Figure 2. The particle size analysis of isolated nanocellulose displayed alterations post-supercritical treatment; the control group exhibited the highest percentage within the 100 to 1000 nm range. However, high-pressure and low-temperature treatment proved more efficient, yielding smaller particles compared to those obtained through low-pressure and high-temperature treatment.

Several studies have highlighted the efficacy of supercritical treatment in reducing particle size [5, 23]. This treatment method has been recognized for its capacity to modify the morphology and size of nanocellulose [24]. By manipulating parameters like temperature, pressure, and treatment duration within supercritical fluid treatment, precise control over particle size and desired modifications can be achieved. In our study, both HPLT and LPHT groups subjected to supercritical treatment displayed smaller particle sizes compared to the control group. The  $\text{scCO}_2$

treatment involves using  $\text{scCO}_2$  to eliminate impurities and alter natural fiber properties. This treatment enables  $\text{scCO}_2$  to penetrate fibers, leading to fiber fractionation and increased sensitivity to the acid hydrolysis process.

The mechanism of  $\text{scCO}_2$  treatment in reducing the particle size of nanocellulose involves a combination of factors, including the solvation and plasticization of cellulose, the disruption of cellulose aggregates, and the subsequent precipitation or recrystallization of nanocellulose. When cellulose is exposed to  $\text{scCO}_2$ , the  $\text{CO}_2$  molecules can penetrate the amorphous regions of cellulose and solvate the polymer chains. This solvation process leads to the plasticization of cellulose, making it more flexible and susceptible to deformation [25]. The plasticized cellulose can then undergo structural rearrangements and disruptions.  $\text{scCO}_2$  can also cause the disruption of cellulose aggregates by penetrating into the interstitial spaces between the cellulose nanocrystals or nanofibrils, which can be seen in XRD results. This infiltration leads to the separation and dispersion of the cellulose particles, effectively reducing their agglomeration and size. The solvating effect of  $\text{CO}_2$  also weakens the intermolecular forces between

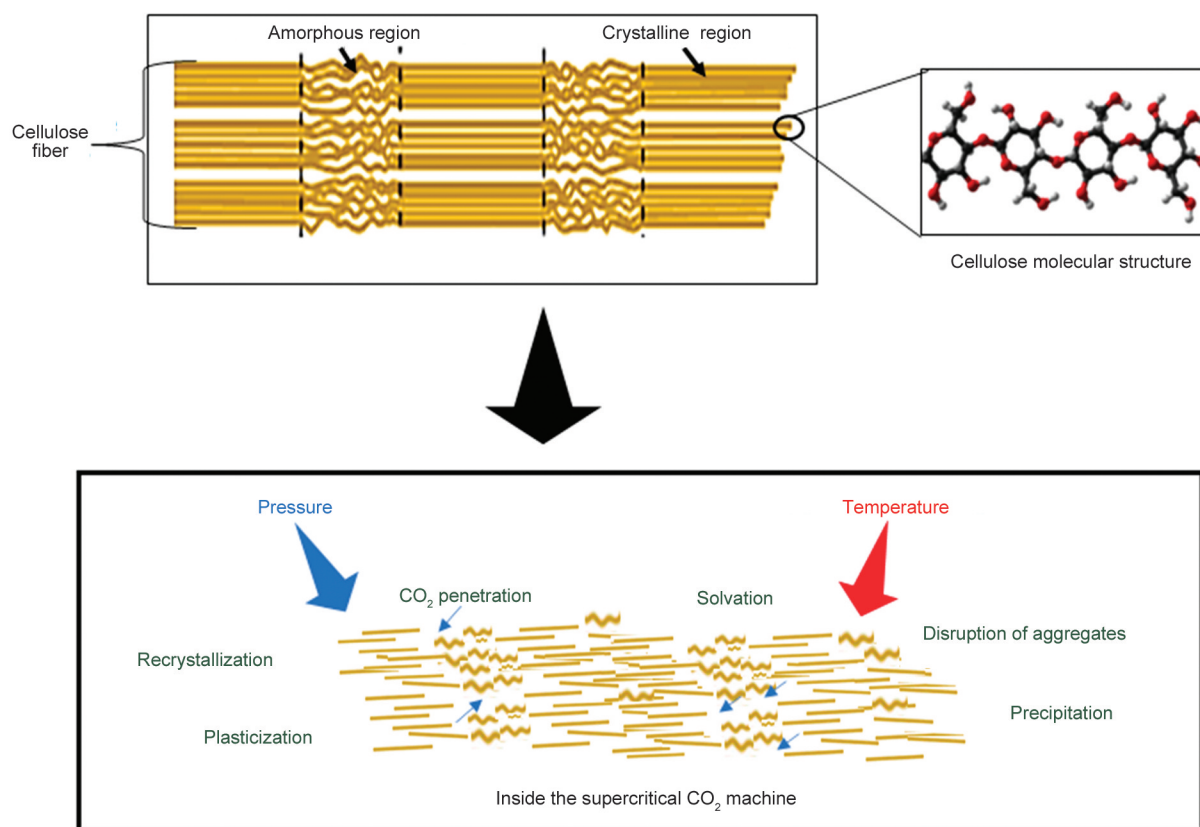


**Figure 3.** The mechanism of supercritical carbon dioxide in reducing the particle size of nanocellulose.

cellulose particles, facilitating their individualization [26]. Furthermore, as the  $\text{scCO}_2$  treatment proceeds, the dissolved cellulose in the supercritical fluid can undergo a precipitation or recrystallization process upon depressurization or cooling. This precipitation or recrystallization can lead to the formation of smaller and more uniform nanocellulose particles (Figure 2b).

Overall, the combination of solvation, plasticization, disruption of aggregates, and precipitation or recrystallization processes contributes to the reduction in particle size of nanocellulose during  $\text{scCO}_2$  treatment. Figure 3 illustrates the mechanism of  $\text{scCO}_2$  treatment in reducing the particle size of nanocellulose. Figure 2c presents the FTIR spectra of the three groups in which we can see the similarity between the two treated group and the slightly different between them and the control group. Broad peak and great intensity in the  $-\text{OH}$  stretch can be clearly seen in the three groups at the range between  $3000\text{--}3800\text{ cm}^{-1}$ . The removal of lignin was done two times; during the paper fabrication and during the isolation of nanocellulose, which can be confirmed by decreasing the intensity of the peaks at the range  $1225\text{--}1250\text{ cm}^{-1}$  [27].

XRD was done to analyze the diffraction pattern of the materials and check for any potential change that may occur during supercritical treatment [28]. Figure 2d show the XRD graphs in which no significant difference can be observed; crystallinity index analysis for the three groups showed that control group had 77.3%, which supercritical treated groups had 78.2 and 77.9% for the HPLT and LPHT groups respectively. The crystallinity index is a measure of the relative amount of crystalline material in a sample compared to the total cellulose content [29]. It is determined by comparing the intensity of the crystalline peaks in the XRD pattern with the intensity of the amorphous background. Our isolated samples showed mostly similar diffraction peaks that represents the typical cellulose I diffraction peaks [30]. The zeta potential of nanocellulose samples refers to the electric potential difference at the interface between the nanocellulose particles and the surrounding medium [31]. It provides information about the surface charge and stability of nanocellulose dispersions. HPLT nanocellulose gives the greatest negative zeta potential values:  $-32.4 \pm 4.01\text{ mV}$  showing that these nano fibers were in a more stable dispersed state compared to other samples that showed smaller

zeta potential of  $26.0 \pm 2.34$  and  $25.9 \pm 3.13\text{ mV}$  for LPHT and C group respectively. When nanocellulose particles are dispersed in a liquid medium, they can acquire a net electric charge due to the dissociation of surface functional groups, such as hydroxyl  $-\text{OH}$  groups, which can ionize to release charged species. The high zeta potential of HPLT sample indicates a high surface charge compared with the control sample, resulting in electrostatic repulsion between the particles. This repulsion helps to prevent particle aggregation and promotes the stability of the dispersion [32]. On the other hand, the control sample with lower zeta potential may lead to more particle aggregation and instability. It has been reported that the zeta potential of cellulose nanofibers (CNF) can vary depending on the source of the CNF, the preparation method, and the surrounding environment [33, 34]. However, in general, cellulose nanofibers tends to have a negative zeta potential due to the presence of carboxyl and hydroxyl groups on their surface. Studies have reported zeta potentials for nanocellulose ranging from approximately  $-25$  to  $-60\text{ mV}$  in water at neutral pH [35, 36].

The exact value can depend on several factors such as the degree of fibrillation, the type of cellulose source material, and the presence of any surface modifications. High pressure could modify the fibrillation in the nano fibers and those higher zeta potential appeared in HPLT group of nanocellulose. It's worth noting that the zeta potential of nanocellulose can play an important role in their behavior and stability in aqueous suspensions. A higher negative zeta potential can indicate greater stability due to increased repulsion between particles. Conversely, a lower zeta potential can lead to aggregation and sedimentation of nanocellulose. Thermal properties of the isolated nanocellulose were studied by TGA analysis. Table 1 presents the results of thermal properties of the three samples. The degradation temperatures ( $T_{\text{max}}$ ) as shown in the table for the C, HPLT and LPHT group were found at  $321.7 \pm 2.3$ ,  $338.0 \pm 3.7$  and  $330.2 \pm 4.0^\circ\text{C}$ , respectively. These findings higher than those obtained by Romruen *et al.* [37], who isolated nanocellulose from different agricultural wastes. Upon the exposure of nanocellulose to high temperatures, nanocellulose undergo thermal degradation, which lead to weight loss. The extent of weight loss depends on several factors, including the temperature, the duration of exposure, and the type of nanocellulose.

**Table 1.** The results of thermal properties of isolated nanocellulose groups (mean±SD).

Nanocellulose		C group	HPLT group	LPHT group
Decomposition temperature [°C]	$T_{\text{onset}}$	287.7±1.8	309.8±3.6	304.9±3.9
	$T_{\text{max}}$	321.6±2.3	338.0±3.7	330.2±4.0
Weight loss [%]	100 °C	7.2±0.4	6.9±0.1	6.0±0.4
	200 °C	19.3±0.8	17.2±0.2	16.9±0.7
	400 °C	47.8±1.3	44.7±1.4	45.2±0.9
	600 °C	83.0±3.0	79.1±1.9	80.9±2.6
	800 °C	88.6±2.8	87.2±3.4	86.8±2.7

The presence of small variance between HPLT and LPHT groups indicates the composition similarity and thermal stability of these groups compared with C group. The initial weight loss of all the three samples took place at around 100 °C, which could be due to the evaporation of moisture and volatile chemicals [38]. In intermediate temperature at a range between 200 and 300 °C, decomposition of hemicelluloses and lignin are occurred. However, owing to the strong cellulose structure, it can endure higher-temperature conditions [39]. Thus, the residue of nanocellulose at higher temperature was different at different groups, which can be explained by the variations in chemical structure and crystallinity [40]. Our thermal analysis findings were consistent with the isolated nanocellulose from different biomass [41, 42].

### 3.2. Characterization of bioaerogel scaffolds

Bioaerogel scaffolds were fabricated by using different concentrations of HPLT group nanocellulose, which was chosen as the best among the other two types. Table 2 presents the results of physical observation of 4 bioaerogel scaffolds prepared with 1, 1.5, 2 and 2.5% of the selected nanocellulose. Owing to the tremendous amount of hydrogen bond on the surface of cellulose nano fibers, they are entangled with each other, which explain the uniform structure and fiber bundles in the pure CNFs aerogel. These organized bundles are responsible for the high porosity, good structure and performance of CNFs aerogel [43]. Another final factor affecting the porosity of

aerogels, with additives such as fillers or any other material may alter the architecture of the aerogel's porosity [43]. Figure 4 presents the morphological analysis of the fabricated bioaerogel scaffolds in which can be seen that the nanocellulose forms a porous and sponge-like structure, which contributes to the aerogel's exceptional lightweight and high surface area characteristics. BAS1 and BAS1.5 had the largest pore size and thus the lowest porosity compared with the other two samples. The surface of the four samples looks the same since the same source of nanocellulose and same approach were used in the fabrication process. Our finding support those obtained in previous studies for bioaerogels with a porosity higher than 99%, stated that bioaerogel density inversely proportional to its porosity and directly proportional to the precursor material initial concentration [44, 45]. The SEM images highlight the presence of numerous pores throughout the aerogel's structure. These pores are a result of the interconnected nanocellulose fibers or particles leaving void spaces between them during the fabrication process. Table 2 presents the physical characteristics of the bioaerogel scaffolds including the density, porosity, water absorption, pore size and surface area. The density of the aerogels ranged from 7.7±0.8 (BAS1) to 15.0±0.4 mg/cm<sup>3</sup> (BAS2.5), while porosity of the bioaerogels ranged from 98.6±0.7 to 99.3±0.8%. The density of aerogel was found to be inversely related to the porosity and directly proportional to the initial concentration of the nanocellulose, which support the results of several previous studies [46, 47]. The density and porosity of nanocellulose aerogels can vary based on several factors, including the preparation method, source of nanocellulose, and the specific drying technique used [48]. Since the same material and same preparation were used in the present study, it can be clearly seen the effect of the material concentration on the physical properties. The pore size of a nanocellulose aerogel is an important parameter that affects its physical and chemical properties, including its mechanical strength, thermal

**Table 2.** Fabrication of bioaerogel scaffolds using different concentrations of nanocellulose.

Bioaerogel sample	Density [mg/cm <sup>3</sup> ]	Porosity [%]	Water absorption [g/g]	Average pore size [μm]	Surface area [m <sup>2</sup> /g]
BAS1	7.7±0.8	98.9±0.7	16.4±3.5	131.9±6.2	48.3±3.2
BAS1.5	9.8±0.3	99.1±1.2	19.1±6.2	63.8±5.1	90.8±5.8
BAS2	13.2±0.6	99.3±0.8	35.9±5.2	23.0±4.7	139.1±5.8
BAS2.5	15.0±0.4	99.4±0.6	38.3±8.4	14.0±2.3	181.6±6.9



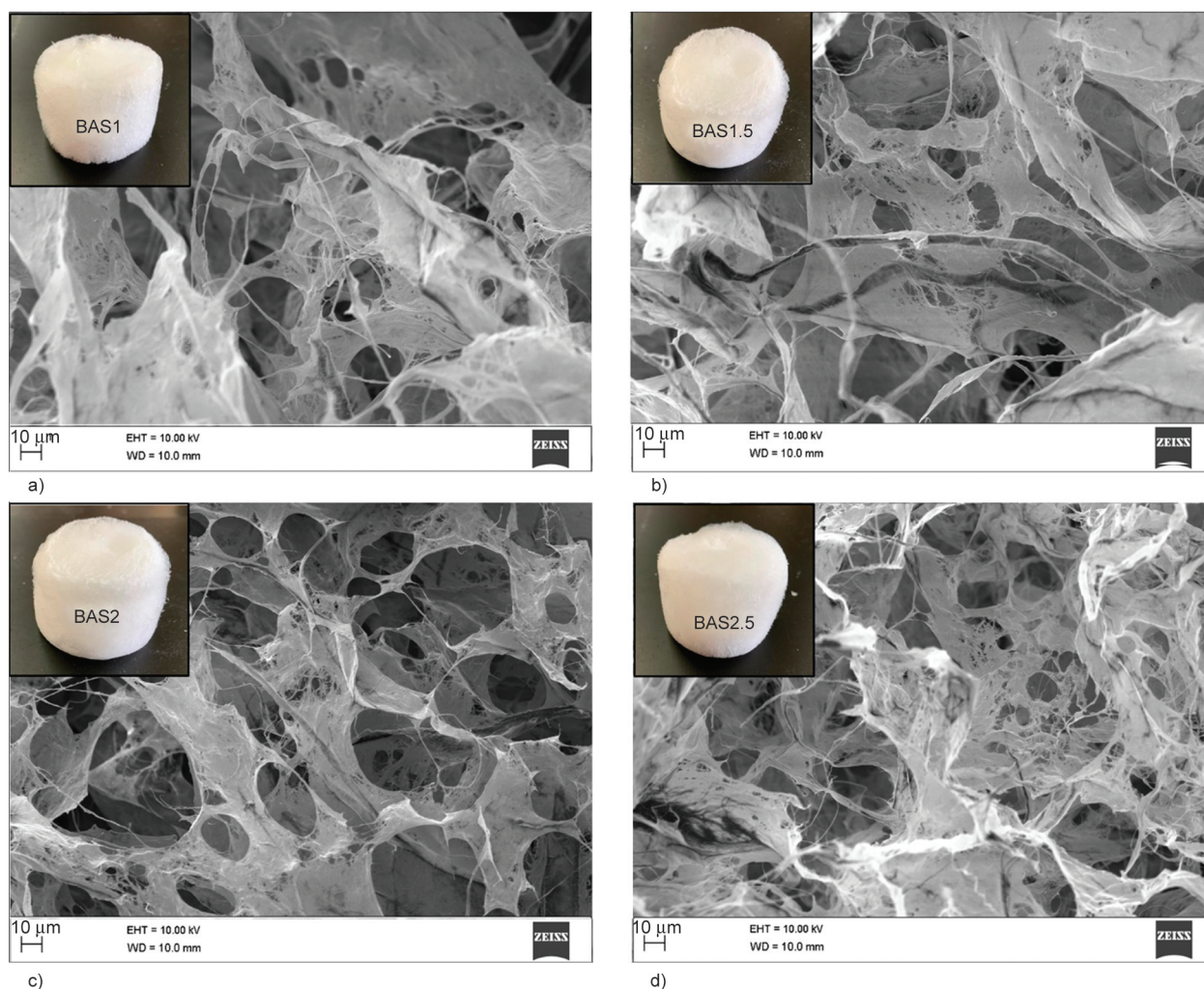


**Figure 4.** Scanning electron microscopy (SEM) analysis for prepared bioaerogels samples at similar magnification (400×). a) SEM image for sample BAS1, prepared with 1% concentration of nanocellulose, b) SEM image for sample BAS1.5, c) SEM image for sample BAS2, and d) SEM image for sample BAS2.5.

insulation, and sorption capacity [49]. in the present study, the smallest average pore size was reported for sample BAS2.5 ( $14 \pm 2.3$ ), the higher the porosity the smaller pore size and higher surface area of the aerogel. As a highly hydrophilic material, the higher the concentration of nanocellulose the higher water absorption of the bioaerogel scaffold.

Depending on the material prepared from, aerogels tend to be sensitive to moisture absorption from handling and storage, and more brittle with aging and may exhibit stress relaxation (or creep) under certain conditions. Morphology and pore size of aerogels is typically influenced by many factors which include precursor material, preparation method, additives materials, cooling rate, and physical conditions. It has been reported that supercritical drying approach for CNF based aerogels can obtain small and open pores in the aerogel [50]. In order to have small pores with more homogeneity in their structure, a rapid cooling

rate should be applied to the aerogel. As a highly hydrophilic material, CNFs aerogel possessed the highest water absorption value. Owing to the ability of  $\text{CO}_2$  to penetrate into the fiber structure and cause swelling, which can lead to an increase in surface area and pore size and thus enhance the water absorption performance [23]. Figure 5a presents the results of thermal analysis of bioaerogel samples, in which can be seen that the samples prepared using higher concentrations (BAS2.5) showed better thermal stability compared with the lower ones. However, FT-IR and XRD analysis showed similar spectra for the four samples (Figures 5b and 5c).

The outcomes from the texture profile analysis of the bioaerogel scaffolds, depicted in Figure 5d, demonstrate a substantial enhancement in various parameters strength, resilience, cohesiveness, and springiness as the concentration of nanocellulose in the samples increases. Nanocellulose aerogels exhibit



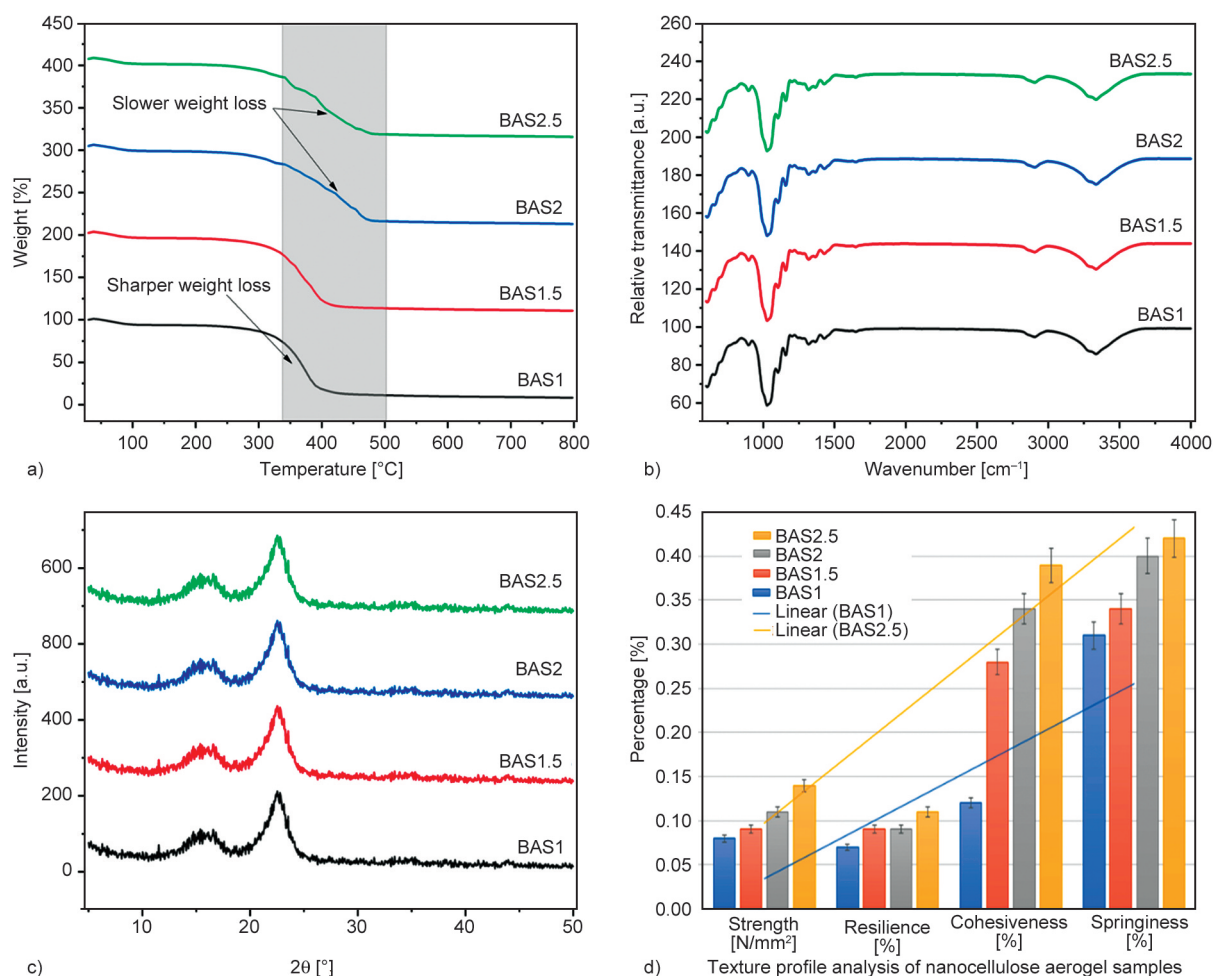


**Figure 5.** Characterization of bioaerogel scaffolds; a) TGA analysis, b) FT-IR spectra, c) XRD analysis and d) texture profile analysis.

impressive strength-to-weight ratios despite their low density, owing to their hierarchical structure composed of interconnected nanofibrils [51]. The robust intermolecular interactions within these nanofibrils significantly contribute to the aerogel's overall strength [52]. In this study, BAS1 displayed the lowest mechanical values among the samples, exhibiting a strength of 0.08 N/mm<sup>2</sup>. Cohesiveness, attributed to strong intermolecular hydrogen bonding in nanocellulose chains, ensures structural integrity and prevents collapse under external loads. All samples demonstrated good springiness, showcasing elastic behavior capable of withstanding deformation and recovering their shape upon force removal. These findings underscore the versatility of nanocellulose aerogels across diverse applications, including lightweight structural materials, biomedical devices, and energy storage systems.

#### 4. Conclusions

The study successfully demonstrated the potential of isolating nanocellulose from oil palm empty fruit bunch fibers using 50% fewer chemicals, aided by scCO<sub>2</sub> treatment post-bleaching. The application of scCO<sub>2</sub>, pressurized and heated beyond its critical point, facilitated the penetration of natural fibers, effectively reducing nanocellulose particle size. The resultant bioaerogel scaffolds exhibited nanostructures due to smaller particle sizes and well-dispersed suspensions. Nanocellulose concentration significantly influenced density, porosity, pore size, and volume, with higher concentrations correlating to increased porosity and reduced pore size. Mechanical properties and stability of bioaerogels showed a direct correlation with nanocellulose concentration. While all bioaerogel scaffolds displayed high water absorption properties, none retained stability underwater.

Employing a cleaner approach in both nanocellulose isolation and bioaerogel fabrication suggests the potential utilization of these biomaterials across various medical and biomedical applications.

## Acknowledgements

The authors would like to thank the Researchers Supporting Project number (RSP2024R138), King Saud University, Riyadh, Saudi Arabia. The authors would like to thank the collaboration between Universitas Negeri Padang, Indonesia, King Saud University, Riyadh, Saudi Arabia, Florida Institute of Technology, USA and Universiti Sains Malaysia, Penang, Malaysia that has made this work possible

## References

- [1] Suhartini S., Hidayat N., Rohma N. A., Paul R., Panges-tuti M. B., Utami R. N., Nurika I., Melville L.: Sustainable strategies for anaerobic digestion of oil palm empty fruit bunches in Indonesia: A review. *International Journal of Sustainable Energy*, **41**, 2044–2096 (2022).  
<https://doi.org/10.1080/14786451.2022.2130923>
- [2] O'Connor J., Skeaff S., Bremer P., Lucci G., Miroso M.: A critical review of on-farm food loss and waste: Future research and policy recommendations. *Renewable Agriculture and Food Systems*, **38**, e24 (2023).  
<https://doi.org/10.1017/S1742170523000169>
- [3] Septevani A. A., Rifathin A., Sari A. A., Sampora Y., Ariani G. N., Sudiarmanto, Sondari D.: Oil palm empty fruit bunch-based nanocellulose as a super-adsorbent for water remediation. *Carbohydrate Polymers*, **229**, 115433 (2020).  
<https://doi.org/10.1016/j.carbpol.2019.115433>
- [4] Iskandar M. A., Yahya E. B., Abdul Khalil H. P. S., Rahman A. A., Ismail M. A.: Recent progress in modification strategies of nanocellulose-based aerogels for oil absorption application. *Polymers*, **14**, 849 (2022).  
<https://doi.org/10.3390/polym14050849>
- [5] Rizal S., Yahya E. B., Abdul Khalil H. P. S., Abdullah C. K., Marwan M., Ikramullah I., Muksin U.: Preparation and characterization of nanocellulose/chitosan aerogel scaffolds using chemical-free approach. *Gels*, **7**, 246 (2021).  
<https://doi.org/10.3390/gels7040246>
- [6] Abdul Khalil H. P. S., Yahya E. B., Tajarudin H. A., Surya I., Muhammad S., Fazita M. N.: Enhancing the properties of industrial waste nanocellulose bioaerogels using turmeric nano particles. *Industrial Crops and Products*, **197**, 116500 (2023).  
<https://doi.org/10.1016/j.indcrop.2023.116500>
- [7] Marakana P. G., Dey A., Saini B.: Isolation of nanocellulose from lignocellulosic biomass: Synthesis, characterization, modification, and potential applications. *Journal of Environmental Chemical Engineering*, **9**, 106606 (2021).  
<https://doi.org/10.1016/j.jece.2021.106606>
- [8] Zhang L., Liao Y., Wang Y.-C., Zhang S., Yang W., Pan X., Wang Z. L.: Cellulose II aerogel-based triboelectric nanogenerator. *Advanced Functional Materials*, **30**, 2001763 (2020).  
<https://doi.org/10.1002/adfm.202001763>
- [9] Qin H., Zhang Y., Jiang J., Wang L., Song M., Bi R., Zhu P., Jiang F.: Multifunctional superelastic cellulose nanofibrils aerogel by dual ice-templating assembly. *Advanced Functional Materials*, **31**, 2106269 (2021).  
<https://doi.org/10.1002/adfm.202106269>
- [10] Yahya E. B., Jummaat F., Amirul A. A., Adnan A. A., Olaiya N. G., Abdullah C. K., Rizal S., Haafiz M. K. M., Abdul Khalil H. P. S.: A review on revolutionary natural biopolymer-based aerogels for antibacterial delivery. *Antibiotics*, **9**, 648 (2020).  
<https://doi.org/10.3390/antibiotics9100648>
- [11] Abdul Khalil H. P. S., Yahya E. B., Jummaat F., Adnan A. S., Olaiya N. G., Rizal S., Abdullah C. K., Pasquini D., Thomas S.: Biopolymers based aerogels: A review on revolutionary solutions for smart therapeutics delivery. *Progress in Materials Science*, **131**, 101014 (2022).  
<https://doi.org/10.1016/j.pmatsci.2022.101014>
- [12] Saleh W. M., Ahmad M. I., Yahya E. B., Abdul Khalil H. P. S.: Nanostructured bioaerogels as a potential solution for particulate matter pollution. *Gels*, **9**, 575 (2023).  
<https://doi.org/10.3390/gels9070575>
- [13] Gao J., Wang J., Cai M., Xu Q., Zhang J., Cao X., Zhang J., Chen Y.: Advanced superhydrophobic and multifunctional nanocellulose aerogels for oil/water separation: A review. *Carbohydrate Polymers*, **300**, 120242 (2022).  
<https://doi.org/10.1016/j.carbpol.2022.120242>
- [14] Khair F. N. M., Masrol S. R.: The characteristics of pulp and paper made from top section of betong (*Dendrocalamus asper*) bamboo by soda pulping method. *Progress in Engineering Application and Technology*, **3**, 849–857 (2022).  
<https://doi.org/10.30880/peat.2022.03.01.084>
- [15] Wise L. E., Murphy M., Adieco A. A. D.: Chlorite holo-cellulose, its fractionation and bearing on summative wood analysis and on studies on the hemicelluloses. *Paper Trade Journal*, **122**, 35–43 (1946).
- [16] Atiqah M. S. N., Gopakumar D. A., Owolabi F. A. T., Pottathara Y. B., Rizal S., Aprilia N. A. S., Hermawan D., Paridah M. T. T., Thomas S., Abdul Khalil H. P. S.: Extraction of cellulose nanofibers *via* eco-friendly supercritical carbon dioxide treatment followed by mild acid hydrolysis and the fabrication of cellulose nanopapers. *Polymers*, **11**, 1813 (2019).  
<https://doi.org/10.3390/polym11111813>
- [17] Yahya E. B., Abdul Khalil H. P. S., Ahmad M. I., Rizal S., Muhammad S.: Cleaner approach of preparing antibacterial bioaerogel scaffolds using oil palm waste nanocellulose. *Industrial Crops and Products*, **191**, 115897 (2023).  
<https://doi.org/10.1016/j.indcrop.2022.115897>

- [18] Peng Y., Gardner D. J., Han Y., Kiziltas A., Cai Z., Tshabalala M. A.: Influence of drying method on the material properties of nanocellulose I: Thermostability and crystallinity. *Cellulose*, **20**, 2379–2392 (2013).  
<https://doi.org/10.1007/s10570-013-0019-z>
- [19] Sai H., Fu R., Xing L., Xiang J., Li Z., Li F., Zhang T.: Surface modification of bacterial cellulose aerogels' web-like skeleton for oil/water separation. *ACS Applied Materials and Interfaces*, **7**, 7373–7381 (2015).  
<https://doi.org/10.1021/acsami.5b00846>
- [20] Ganesh S., Ramakrishnan S. K., Palani V., Sundaram M., Sankaranarayanan N., Ganesan S. P.: Investigation on the mechanical properties of ramie/kenaf fibers under various parameters using GRA and TOPSIS methods. *Polymer Composites*, **43**, 130–143 (2022).  
<https://doi.org/10.1002/pc.26362>
- [21] Samir A., Ashour F. H., Hakim A. A. A., Bassyouni M.: Recent advances in biodegradable polymers for sustainable applications. *npj Materials Degradation*, **6**, 68 (2022).  
<https://doi.org/10.1038/s41529-022-00277-7>
- [22] Segato F., Damásio A. R., de Lucas R. C., Squina F. M., Prade R. A.: Genomics review of holocellulose deconstruction by aspergilli. *Microbiology and Molecular Biology Reviews*, **78**, 588–613 (2014).  
<https://doi.org/10.1128/mmr.00019-14>
- [23] Nasution H., Yahya E. B., Abdul Khalil H. P. S., Shaah M. A., Suriani A. B., Mohamed A., Alfatah T., Abdullah K. C.: Extraction and isolation of cellulose nanofibers from carpet wastes using supercritical carbon dioxide approach. *Polymers*, **14**, 326 (2022).  
<https://doi.org/10.3390/polym14020326>
- [24] Buffiere J.: Low-molecular-weight nanocellulose produced using supercritical water treatment. Aalto University Publication Series, Aalto (2020).
- [25] Nasution H., Yahya E. B., Abdul Khalil H. P. S., Shaah M. A., Suriani A. B., Mohamed A., Alfatah T., Abdullah C. K.: Extraction and isolation of cellulose nanofibers from carpet wastes using supercritical carbon dioxide approach. *Polymers*, **14**, 326 (2022).  
<https://doi.org/10.3390/polym14020326>
- [26] Li L., Zhuang J., Zou H., Pang J., Yu S.: Partition usage of cellulose by coupling approach of supercritical carbon dioxide and cellulase to reducing sugar and nanocellulose. *Carbohydrate Polymers*, **229**, 115533 (2020).  
<https://doi.org/10.1016/j.carbpol.2019.115533>
- [27] Zheng D., Zhang Y., Guo Y., Yue J.: Isolation and characterization of nanocellulose with a novel shape from walnut (*Juglans regia* L.) shell agricultural waste. *Polymers*, **11**, 1130 (2019).  
<https://doi.org/10.3390/polym11071130>
- [28] Babicka M., Woźniak M., Dwiecki K., Borysiak S., Ratajczak I.: Preparation of nanocellulose using ionic liquids: 1-propyl-3-methylimidazolium chloride and 1-ethyl-3-methylimidazolium chloride. *Molecules*, **25**, 1544 (2020).  
<https://doi.org/10.3390/molecules25071544>
- [29] Madhushani W. H., Priyadarshana R. W. I. B., Ranawana S. R. W. M. C. J. K., Senarathna K. G. C., Kaliyadasa P. E.: Determining the crystallinity index of cellulose in chemically and mechanically extracted banana fiber for the synthesis of nanocellulose. *Journal of Natural Fibers*, **19**, 7973–7981 (2022).  
<https://doi.org/10.1080/15440478.2021.1958428>
- [30] Gopakumar D. A., Pasquini D., Henrique M. A., de Moraes L. C., Grohens Y., Thomas S.: Meldrum's acid modified cellulose nanofiber-based polyvinylidene fluoride microfiltration membrane for dye water treatment and nanoparticle removal. *ACS Sustainable Chemistry and Engineering*, **5**, 2026–2033 (2017).  
<https://doi.org/10.1021/acssuschemeng.6b02952>
- [31] Solhi L., Guccini V., Heise K., Solala I., Niinivaara E., Xu W., Mihhels K., Kröger M., Meng Z., Wohler J., Tao H., Cranson E. D., Kontturi E.: Understanding nanocellulose–water interactions: Turning a detriment into an asset. *Chemical Reviews*, **123**, 1925–2015 (2023).  
<https://doi.org/10.1021/acs.chemrev.2c00611>
- [32] Aguado R. J., Mazega A., Tarrés Q., Delgado-Aguilar M.: The role of electrostatic interactions of anionic and cationic cellulose derivatives for industrial applications: A critical review. *Industrial Crops and Products*, **201**, 116898 (2023).  
<https://doi.org/10.1016/j.indcrop.2023.116898>
- [33] Sim K., Lee J., Lee H., Youn H. J.: Flocculation behavior of cellulose nanofibrils under different salt conditions and its impact on network strength and dewatering ability. *Cellulose*, **22**, 3689–3700 (2015).  
<https://doi.org/10.1007/s10570-015-0784-y>
- [34] Miao X., Lin J., Bian F.: Utilization of discarded crop straw to produce cellulose nanofibrils and their assemblies. *Journal of Bioresources and Bioproducts*, **5**, 26–36 (2020).  
<https://doi.org/10.1016/j.jobab.2020.03.003>
- [35] Weiji W.: Development and characteristics of a high temperature environmentally friendly nanocellulose filter loss reducer (in Chinese). *Drilling Fluid and Completion Fluid*, **37**, 421–426 (2020).  
<https://doi.org/10.3969/j.issn.1001-5620.2020.04.003>
- [36] Mikhaylov V. I., Torlopov M. A., Krivoschapkina E. F., Martakov I. S., Krivoschapkin P. V.: Heteroaggregation of cellulose nanocrystals with Fe<sub>2</sub>O<sub>3</sub> nanoparticles. *Journal of Sol-Gel Science and Technology*, **88**, 6–12 (2018).  
<https://doi.org/10.1007/s10971-017-4374-3>
- [37] Romruen O., Kaewprachu P., Karbowiak T., Rawdkuen S.: Isolation and characterization cellulose nanosphere from different agricultural by-products. *Polymers*, **14**, 2534 (2022).  
<https://doi.org/10.3390/polym14132534>
- [38] Merci A., Urbano A., Grossmann M. V. E., Tischer C. A., Mali S.: Properties of microcrystalline cellulose extracted from soybean hulls by reactive extrusion. *Food Research International*, **73**, 38–43 (2015).  
<https://doi.org/10.1016/j.foodres.2015.03.020>



- [39] Bano S., Negi Y. S.: Studies on cellulose nanocrystals isolated from groundnut shells. *Carbohydrate Polymers*, **157**, 1041–1049 (2017).  
<https://doi.org/10.1016/j.carbpol.2016.10.069>
- [40] Jiang F., Hsieh Y.-L.: Chemically and mechanically isolated nanocellulose and their self-assembled structures. *Carbohydrate Polymers*, **95**, 32–40 (2013).  
<https://doi.org/10.1016/j.carbpol.2013.02.022>
- [41] Sasikala M., Umapathy M. J.: Preparation and characterization of pineapple leaf cellulose nanocrystal reinforced gelatin bio-nanocomposite with antibacterial banana leaf extract for application in food packaging. *New Journal of Chemistry*, **42**, 19979–19986 (2018).  
<https://doi.org/10.1039/C8NJ02973C>
- [42] Wang Z., Qiao X., Sun K.: Rice straw cellulose nanofibrils reinforced poly(vinyl alcohol) composite films. *Carbohydrate Polymers*, **197**, 442–450 (2018).  
<https://doi.org/10.1016/j.carbpol.2018.06.025>
- [43] Xiong S., Zhou J., Wu J., Li H., Zhao W., He C., Liu Y., Chen Y., Fu Y., Duan H.: High performance acoustic wave nitrogen dioxide sensor with ultraviolet activated 3D porous architecture of Ag-decorated reduced graphene oxide and polypyrrole aerogel. *ACS Applied Materials and Interfaces*, **13**, 42094–42103 (2021).  
<https://doi.org/10.1021/acsami.1c13309>
- [44] Chen W., Li Q., Wang Y., Yi X., Zeng J., Yu H., Liu Y., Li J.: Comparative study of aerogels obtained from differently prepared nanocellulose fibers. *ChemSusChem*, **7**, 154–161 (2014).  
<https://doi.org/10.1002/cssc.201300950>
- [45] Abdul Khalil H. P. S., Adnan A. S., Yahya E. B., Olaiya N. G., Safrida S., Hossain M. S., Balakrishnan V., Gopakumar D. A., Abdullah C. K., Oyekanmi A. A., Pasquini D.: A review on plant cellulose nanofibre-based aerogels for biomedical applications. *Polymers*, **12**, 1759 (2020).  
<https://doi.org/10.3390/polym12081759>
- [46] Nissilä T., Karhula S. S., Saarakkala S., Oksman K.: Cellulose nanofiber aerogels impregnated with bio-based epoxy using vacuum infusion: Structure, orientation and mechanical properties. *Composites Science and Technology*, **155**, 64–71 (2018).  
<https://doi.org/10.1016/j.compscitech.2017.12.001>
- [47] Kobayashi Y., Saito T., Isogai A.: Aerogels with 3D ordered nanofiber skeletons of liquid-crystalline nanocellulose derivatives as tough and transparent insulators. *Angewandte Chemie International Edition*, **53**, 10394–10397 (2014).  
<https://doi.org/10.1002/anie.201405123>
- [48] Chen Y., Zhou L., Chen L., Duan G., Mei C., Huang C., Han J., Jiang S.: Anisotropic nanocellulose aerogels with ordered structures fabricated by directional freeze-drying for fast liquid transport. *Cellulose*, **26**, 6653–6667 (2019).  
<https://doi.org/10.1007/s10570-019-02557-z>
- [49] Chhajed M., Verma C., Gupta P., Maji P. K.: Multifunctional esterified nanocellulose aerogel: Impact of fatty chain length on oil/water separation and thermal insulation. *Cellulose*, **30**, 1717–1739 (2023).  
<https://doi.org/10.1007/s10570-022-04993-w>
- [50] Wang Z., Zhu W., Huang R., Zhang Y., Jia C., Zhao H., Chen W., Xue Y.: Fabrication and characterization of cellulose nanofiber aerogels prepared via two different drying techniques. *Polymers*, **12**, 2583 (2020).  
<https://doi.org/10.3390/polym12112583>
- [51] Sun Y., Chu Y., Wu W., Xiao H.: Nanocellulose-based lightweight porous materials: A review. *Carbohydrate Polymers*, **255**, 117489 (2021).  
<https://doi.org/10.1016/j.carbpol.2020.117489>
- [52] Zhu G., Isaza L. G., Huang B., Dufresne A.: Multifunctional nanocellulose/carbon nanotube composite aerogels for high-efficiency electromagnetic interference shielding. *ACS Sustainable Chemistry and Engineering*, **10**, 2397–2408 (2022).  
<https://doi.org/10.1021/acssuschemeng.1c07148>